Computing eigenvalues and eigenfunctions of Schrödinger equations using a model reduction approach

Shuangping Li[1], Zhiwen Zhang[2*]

[1] *Program in Applied and Computational Mathematics, Princeton University, New Jersey, USA 08544.*
[2] *Department of Mathematics, University of Hong Kong, Pokfulam Road, Hong Kong SAR.*

Abstract. We present a model reduction approach to construct problem dependent basis functions and compute eigenvalues and eigenfunctions of stationary Schrödinger equations. The basis functions are defined on coarse meshes and obtained through solving an optimization problem. We shall show that the basis functions span a low-dimensional generalized finite element space that accurately preserves the lowermost eigenvalues and eigenfunctions of the stationary Schrödinger equations. Therefore, our method avoids the application of eigenvalue solver on fine-scale discretization and offers considerable savings in solving eigenvalues and eigenfunctions of Schrödinger equations. The construction the basis functions are independent of each other; thus our method is perfectly parallel. We also provide error estimates for the eigenvalues obtained by our new method. Numerical results are presented to demonstrate the accuracy and efficiency of the proposed method, especially Schrödinger equations with double well potentials are tested.

1 Introduction

In this paper, we construct a set of problem dependent basis functions to compute eigenvalues and eigenfunctions of Schrödinger equations. To be more specific, we consider the eigenvalue problem of the stationary Schrödinger equation with a potential $V(x)$ of the following form

$$\mathcal{H}u(x) := -\Delta u(x) + V(x)u(x) = \lambda u(x), \quad x \in \Omega \subseteq R^d, \tag{1.1}$$

$$u(x) = 0, \quad x \in \partial\Omega \subseteq R^d, \tag{1.2}$$

Corresponding author. Email addresses: sl31@math.princeton.edu (S. Li), zhangzw@hku.hk (Z. Zhang)

where Ω is a bounded domain in $\mathbb{R}^d$ and $V(x): R^d \to R$ is a real-valued function. λ and $u(x)$ are the corresponding eigenvalues and eigenfunctions of the Hamiltonian operator $\mathcal{H} = -\Delta + V(x)$. We should emphasize that the spectrum of the Hamiltonian operator $\mathcal{H}$ can have negative values and physically the negative part of the spectrum corresponding to bound states and they have many important applications in computational chemistry [6,17,18,29].

The eigenvalue problem of (1.1) in variational form reads: find an eigenvalue λ and its associated eigenfunction $u(x) \in W := H_0^1(\Omega)$ such that

$$a(u,v) := \int_{\Omega} \left(\nabla u(x) \cdot \nabla v(x) + V(x)u(x)v(x)\right)dx = \lambda \int_{\Omega} u(x)v(x)dx = \lambda(u,v), \qquad (1.3)$$

for all $v \in W$. By using the finite element method (FEM), we obtained the discretized problem of the eigenvalue problem (1.3): find λ_h and associated eigenfunctions $u_h(x) \in V_h \subseteq W$ such that

$$a(u_h,v_h) = \lambda_h(u_h,v_h), \quad \text{for all} \quad v_h \in V_h, \qquad (1.4)$$

where V_h is a conforming finite element space spanned by N_h nodal basis functions on some regular finite element mesh $\mathcal{T}_h$ with mesh size h. After the FEM discretization, one could apply eigenvalue algorithms, including QR-algorithm, Lanczos algorithm, and Arnoldi iteration, directly to the N_h-dimensional finite element matrices to obtain the eigen-pairs $\{\lambda_h, u_h\}$, see [10] and references therein. We remark that it is extremely expensive to compute eigenvalues and eigenfunctions of (1.4) when N_h becomes big. For example, finding all eigenvalues and eigenvectors of the matrix corresponding to the FEM discretization of (1.4) using QR-algorithm costs $6N_h^3 + O(N_h^2)$ flops.

In practice, however, we are mainly interested in the first few lowermost eigenvalues and eigenfunctions as they have important meanings in computational chemistry [19]. In addition, when we use the FEM to approximate eigenvalues of (1.4), the number of reliable numerical eigenvalues takes up only a tiny portion of the total degrees of freedom N_h in the resulting discrete system. See [2, 30–32, 35] for the discussion of second-order elliptic eigenvalue problems.

This motivates us to avoid the application of eigenvalue algorithms for the fine-scale FEM discretization (1.4) and build a low-dimensional generalized finite element space so that we can accurately and efficiently compute the lowermost eigenvalues and eigenfunctions. Specifically, we introduce a coarse discretization of the physical space Ω into mesh $\mathcal{T}_H$ with mesh size $H \gg h$. On the coarse mesh $\mathcal{T}_H$, we build a set of basis functions $\{\Psi_i(x)\}_{i=1}^{N_H}$ that generate a low-dimensional generalized finite element space V_c. The dimension of V_c is N_H and it is much smaller than N_h. In the low-dimensional space V_c, we compute the discretized form of the eigenvalue problem (1.3): find λ_H and associated eigenfunctions $u_H(x) \in V_c \subseteq W$ such that

$$a(u_H,v_H) = \lambda_H(u_H,v_H) \quad \text{for all} \quad v_H \in V_c, \qquad (1.5)$$

The basis functions $\{\Psi_i\}_{i=1}^{N_H}$ have already captured the information of the Schrödinger equation, which enables us to accurately compute the first few important eigen-pairs of (1.1), $\{\lambda_H, u_H\}$. The construction of the basis functions $\{\Psi_i\}_{i=1}^{N_H}$ involves solving of N_H optimization problems [4]. These optimization problems are independent of each other and thus can be computed in parallel. Recall that the size of the matrix obtained by the discretization of (1.5) is N_H. This significantly reduces the computational cost in computing the eigenvalues and eigenfunctions of Schrödinger equation (1.1).

We should point out that the idea of using two-level technique or multi-level technique for designing algorithms for eigenvalue problem and other problems is not new. In [33], a two-grid discretization scheme was proposed to solve eigenvalue problems, including both partial differential equations and integral equations. In [13], Hackbusch proposed a multi-grid method to compute eigenvalues and eigenfunctions of the elliptic problem obtained by the finite element discretization. In [21], Peterseim used the numerical upscaling techniques to compute eigenvalues for a class of linear second-order self-adjoint elliptic partial differential operators. Using similar methodology to construct low-dimensional generalized finite element spaces is pioneered by the generalized finite element method (GFEM) [1] and the multiscale finite element method (MsFEM) [11, 14, 15], and is pervasive in the recent developments in the numerical methods for multiscale problems and elliptic PDEs with random coefficients, see [8, 34] and references therein.

We would like to point out some similarities and differences between our approach and other existing methods. Our construction of basis functions is inspired by the recently development in building localized basis function for multiscale elliptic PDEs and Schrödinger equations, see [16, 20, 21, 23] and reference therein. Previous researchers have utilized the Clément-type quasi-interpolation approach or optimization approach to construct localized basis functions that give optimal approximation property of the elliptic operator. In the Schrödinger equation (1.1), however, the potential $V(x)$ is a real-valued function. Therefore, the Hamiltonian operator $-\Delta + V(x)$ is not necessarily positive definite, which is quite common in Schrödinger equation models, see [12, 28]. We shall construct basis functions that can be used to compress or upscale the Hamiltonian operator in Schrödinger equation (1.1) so that we can compute the corresponding eigen-pairs in the reduced space. In addition, we shall estimate the error of the eigenvalues $|\lambda_h - \lambda_H|$ obtained by the FEM and our new method. We comment that similar ideas of computing eigenvalue problems using adaptive basis functions are considered in [24, 25], though the main point of these papers are different and they mainly focus on numerical investigation. Their goals are to obtain compressed modes that are sparse and spatially localized so they can be used to span the low-energy eigenspace of differential operators.

The rest of the paper is organized as follows. In Section 2, we give a brief introduction of the eigenvalue problems of the Schrödinger equation and its finite element method discretization. In section 3, we present the derivation of basis functions based on the two-scale decompositions and the approximation of eigenvalues and eigenfunctions in the reduced space. Issues regarding the practical implementation of our method will also

be discussed. Error estimate of the eigenvalues and computational complexity analysis will be discussed in Section 4. In Section 5, we present numerical results to demonstrate the accuracy and efficiency of our method. Concluding remarks are made in Section 6.

To simplify the notation, we will write $a \lesssim b$ for two positive quantities a and b, if $a \leq Cb$ with some constant $C > 0$ that depends only on the size of the domain Ω, parameters in Schrödinger equation, and parameters that measures the quality of the underlying finite element mesh. We emphasize that C does not depend on the mesh size h and H.

2 Model problem and its finite element discretization

We compute the eigenpairs $\{\lambda, u(x)\}$ of the following Schrödinger equation on the bounded domain Ω,

$$-\Delta u(x) + V(x)u(x) = \lambda u(x), \quad x \in \Omega \subseteq R^d, \tag{2.1}$$

$$u(x) = 0, \quad x \in \partial\Omega \subseteq R^d. \tag{2.2}$$

The eigenvalue problem of (2.1) in variational form reads: find an eigenvalue λ and its associated eigenfunction $u(x) \in W := H_0^1(\Omega)$ such that

$$a(u,v) := \int_\Omega \left(\nabla u \cdot \nabla v + Vuv\right) dx = \lambda \int_\Omega uv dx = \lambda(u,v), \text{ for all } v \in W, \tag{2.3}$$

In the finite element method, we first partition the physical domain Ω into a set of regular fine elements with mesh size h. For example, we divide Ω into a set of non-overlapping triangles $\mathcal{T}_h = \{\tau_e\}_{e=1}^{N_e}$ such that no vertex of one triangle lies in the interior of the edge of another triangle, where N_e is the number of finite elements. Let $\mathcal{N}_f$ denote the set of interior vertices of $\mathcal{T}_h$. Let N_h denote the number of the interior vertices, which is also equal to the dimension of the finite element space. For every vertex $x_i \in \mathcal{N}_f$, let $\varphi_i(x)$ denote the corresponding nodal basis function, i.e., $\varphi_i(x_j) = \delta_{ij}$, $x_j \in \mathcal{N}_f$. In this paper, we assume that all the nodal basis functions $\varphi_i(x)$ are linear functions and continuous across the boundaries of the elements, so we obtain the first-order conforming finite element space corresponding to $\mathcal{T}_h$,

$$V_h = \{\varphi(x) | \; \forall \tau_e \in \mathcal{T}_h, \; \varphi(x)|_{\tau_e} \text{ is a polynomial of total degree} \leq 1\} \subset H_0^1(\Omega). \tag{2.4}$$

Then, we apply the Galerkin method to solve (2.3). Specifically, we find λ_h and associated eigenfunctions $u_h(x) = \sum_{i=1}^{N_h} u_i \varphi_i(x) \in V_h$ such that

$$a(u_h, v_h) = \lambda_h(u_h, v_h) \quad \text{for all} \quad v_h \in V_h. \tag{2.5}$$

Finally, we solve a generalized eigenvalue problem obtained from the discretization of (2.5) to obtain λ_h and $u_h(x)$. The Hamiltonian operator $-\Delta + V(x)$ is self-adjoint so the eigenvalues are real. They can be sorted in ascending order,

$$\lambda_h^{(1)} \leq \lambda_h^{(2)} \leq \lambda_h^{(3)} \leq \lambda_h^{(4)} \leq \cdots \tag{2.6}$$

If the potential $V(x)$ is bounded from below, we have the estimate for the lowermost eigenvalue $\lambda_h^{(1)}$.

Lemma 2.1. *We assume the potential $V(x) \geq V_{min}$, $\forall x \in \Omega$, then the lowermost eigenvalue $\lambda_h^{(1)}$ is bounded from below.*

Proof. We introduce the *Rayleigh quotient* [30] within the finite dimension subspace V_h, which is defined by

$$R(v_h) = \frac{a(v_h, v_h)}{(v_h, v_h)}, \quad \text{for all} \quad v_h \in V_h, \tag{2.7}$$

Then, $\lambda_h^{(1)} = \min R(v_h)$, $v_h \in V_h$. Obviously, $\lambda_h^{(1)}$ is bounded from below if $V(x) \geq V_{min}$, $\forall x \in \Omega$. In addition, its corresponding eigenfunctions $u_h^{(1)}(x)$ is the critical point of $R(v_h)$ over the finite element space V_h. $\qquad \square$

Remark 2.1. The Rayleigh quotient provides an alternative way to compute eigenvalues and eigenfunctions of the Schrödinger equation (1.1) and its discretized form (2.5) [30]. The l-th eigenvalue is $\lambda_h^{(l)} = \min_{v_h \perp E_{l-1}, v_h \in V_h} R(v_h)$, where E_{l-1} is the eigen-space spanned by eigenfunctions $u_h^1, \cdots, u_h^{l-1}$ associated with eigenvalues $\lambda_h^{(1)}, \cdots, \lambda_h^{(l-1)}$.

In the finite element method framework, the dimension of the discretized problem is proportional to the number of interior vertices in the fine mesh $\mathcal{T}_h$. Therefore, the finite element method becomes expensive for 2D and 3D Schrödinger equations. It is desirable to develop model reduction methods that can efficiently and accurately solve the eigenvalue problem of Schrödinger equation with relatively small computational cost.

3 Construction of basis functions and their corresponding low-dimensional space

In this section, we shall apply the two-level techniques and decompose the finite element space V_h into coarse and fine parts. The coarse part is a low-dimensional generalized finite element space that enables us to efficiently compute the lowermost eigenvalues and eigenfunctions of Schrödinger equations. To achieve this goal, we need to build a set of basis functions $\{\Psi_i(x)\}$ that capture the information of the Hamiltonian operator.

To construct the basis functions $\{\Psi_i(x)\}$, we first partition the physical domain Ω into a set of regular *coarse* elements with mesh size $H \gg h$. Again, we divide Ω into a set of non-overlapping triangles $\mathcal{T}_H = \{T_e\}$ such that no vertex of one triangle lies in the interior of the edge of another triangle. To facilitate the implementation, the fine mesh $\mathcal{T}_h$ and coarse mesh $\mathcal{T}_H$ are nested. Let $\mathcal{N}_c$ denote the set of interior vertices of coarse mesh $\mathcal{T}_H$ and N_H be the number of interior vertices. For every vertex $x_i \in \mathcal{N}_c$, let $\Phi_i(x)$ denote the corresponding FEM nodal basis functions, i.e., $\Phi_i(x_j) = \delta_{ij}$, $x_j \in \mathcal{N}_c$. We also

assume that all the nodal basis functions $\Phi_i(x)$ are continuous across the boundaries of the elements, so we obtain the first-order conforming finite element space corresponding to the coarse mesh $\mathcal{T}_H$,

$$V_H = \{\Phi(x) \mid \forall T_e \in \mathcal{T}_H, \ \Phi(x)|_{T_e} \text{ is a polynomial of total degree} \leq 1\} \subset H_0^1(\Omega). \quad (3.1)$$

The dimension of the coarse finite element space V_H (3.1) is N_H, which is far less than that of fine-scale FEM space V_h. However, one cannot use the coarse finite element basis functions Φ_i, $i = 1,...,N_H$ to directly compute the eigenvalues and eigenfunctions of Schrödinger equation because they do not capture the fine-scale information of the Hamiltonian operator in (1.1). Therefore, we need to construct some problem-dependent basis functions that incorporate the fine-scale information into the coarse finite element space.

In this paper, we construct such basis functions $\{\Psi_i(x)\}_{i=1}^{N_H}$ through an optimization approach [4]. More specifically, we compute the following constrained optimization problem to obtain $\Psi_i(x)$,

$$\Psi_i(x) = \operatorname*{argmin}_{\Psi \in H_0^1(\Omega)} \int_\Omega \left(|\nabla \Psi(x)|^2 + V(x)|\Psi(x)|^2\right) dx \quad (3.2)$$

$$\text{s.t. } \int_\Omega \Psi(x)\Phi_j(x) = \delta_{i,j}, \ \forall 1 \leq j \leq N_H, \quad (3.3)$$

where $\Phi_j(x)$ are the nodal basis functions on the coarse FEM space V_H. The objective function (3.2) contains both the kinetic energy and the potential energy of the Schrödinger equation system. It is important to note that the boundary condition of the Schrödinger equation has already been incorporated in the above optimization problem through the definition of the solution space $H_0^1(\Omega)$. In general, the optimization problem cannot be solved analytically as it is an optimization problem in an infinite dimensional space. We have to solve the optimization problem (3.2)-(3.3) using numerical methods.

In this paper, we apply the finite element method to discretize the basis functions $\Psi_i(x)$. Specifically, we represent $\Psi_i(x) = \sum_{k=1}^{N_h} b_k^{(i)} \varphi_k(x)$, where $\varphi_k(x)$ are the finite element basis functions defined on the fine mesh $\mathcal{T}_h$ and $b_k^{(i)}$'s are the coefficients. In this discrete level, the optimization problem (3.2)-(3.3) is reduced to a constrained quadratic optimization problem, which can be efficiently solved using Lagrange multiplier methods. Since the basis functions are independent of each other, they can be constructed independently and the optimization problem (3.2)-(3.3) can be done perfectly in parallel.

Let V_c denote the conforming generalized finite element space spanned by $\Psi_i(x)$,

$$V_c = \{\Psi_i(x) \mid i = 1,...,N_H\} \subset H_0^1(\Omega). \quad (3.4)$$

Note that the dimension of V_c is equal to the coarse finite element space V_H. However, the basis functions $\Psi_i(x)$ contain fine-scale information of the Hamiltonian operator in (1.1), which enable us to compute the eigenvalue problem (1.3) on the coarse mesh $\mathcal{T}_H$.

Now we use the Galerkin method to solve the eigenvalue problem (1.3) in the generalized finite element space V_c: find $\lambda_H^{(j)}$ and its associated eigenfunctions $u_c^{(j)}(x) \in V_c$, $j = 1, ..., N_H$, such that

$$a(u_c^{(j)}, v) = \lambda_H^{(j)}(u_c^{(j)}, v), \quad \text{for all} \quad v \in V_c. \tag{3.5}$$

In general, the stiffness matrices and mass matrices corresponding to the discretization of (3.5) are not sparse. However, the dimension of the coarse generalized finite element space V_c is $N_H \ll N_h$ so the lack of sparsity is not an issue.

The discrete eigenvalues are ordered in ascending order,

$$\lambda_H^{(1)} \leq \lambda_H^{(2)} \leq \lambda_H^{(3)} \leq \lambda_H^{(4)} \leq \cdots \leq \lambda_H^{(N_H)}. \tag{3.6}$$

Let $u_c^{(j)}$, $j = 1, 2, ..., N_H$ be normalized to one in $L^2(\Omega)$, i.e., $(u_c^{(j)}, u_c^{(j)})_{L^2(\Omega)} = 1$. The discrete eigenfunctions satisfy the orthogonal constraints

$$a(u_c^{(j)}, u_c^{(k)}) = (u_c^{(j)}, u_c^{(k)}) = 0, \, j \neq k. \tag{3.7}$$

4 Errors analysis

In this section, we present the error estimate of the approximate eigenvalues $|\lambda_h - \lambda_H|$ obtained by the finite element method (FEM) and our method. The computational complexity analysis of the FEM and our method can be obtained easily.

4.1 Orthogonal decomposition of the solution space in $L^2(\Omega)$ sense

We first introduce some notations that will be used in the error estimate. Let $V_0 := ||V(x)||_{L^\infty(\Omega)} < +\infty$ and $W := H_0^1(\Omega)$. We define a norm $|||\cdot|||$ to be

$$|||u(x)||| := \sqrt{V_0 ||u||_{L^2(\Omega)}^2 + ||\nabla u||_{L^2(\Omega)}^2}, \text{ for any } u \in W. \tag{4.1}$$

Recall that the bilinear form $a(u, v)$ used in the variational form corresponding to the eigenvalue problem of (1.1) is defined by

$$a(u, v) := (\nabla u, \nabla v) + (Vu, v), \text{ for any } u, v \in W, \tag{4.2}$$

where $V = V(x)$ is the potential function and $(\cdot, \cdot)$ stands for the standard inner product on Ω. Under mild conditions, the second part (Vu, v) in (4.2) can be viewed as a perturbation. Our method requires the following assumption on the resolution of the coarse mesh $\mathcal{T}_H$.

Assumption 4.1. We assume that the potential $V(x)$ is bounded, i.e., $V_0 := ||V(x)||_{L^\infty(\Omega)} < +\infty$, and the mesh size H of $\mathcal{T}_H$ satisfies $H\sqrt{V_0} \lesssim 1$.

Under this assumption, many typical bounded potentials from Schrodinger equation (1.1) can be treated as a perturbation to the kinetic operator. Thus, they can be computed using our method. We also point out that this assumption restrains our ability to handle Schrodinger equation (1.1) with unbounded potential, such as Coulomb potential. We shall consider this issue in our future work.

Before we proceed the error estimate, we first study the orthogonal decomposition of the solution space W. Write V_f as the subset of W defined by

$$V_f = \left\{ v(x) \in W \,\middle|\, \int_\Omega v(x)\Phi_i(x) = 0, \forall i = 1,...,N_H \right\}. \tag{4.3}$$

From the definition of V_f, one can find that V_f contains functions with fine-scale information that cannot be captured by the coarse-scale finite element basis functions $\Phi_i(x)$ defined in (3.1). This property is closely related to the Clément-type interpolation operator [5,9,27]

$$\mathcal{I}_H v(x) := \sum_{x_i \in \mathcal{N}_c} \alpha_i(v)\Phi_i(x), \tag{4.4}$$

where $\mathcal{N}_c$ contains all the interior nodes of coarse mesh, $\Phi_i(x)$ are the nodal basis functions corresponding to x_i, and the quasi-interpolation coefficient $\alpha_i(v)$ is defined by

$$\alpha_i(v) = \frac{\int_\Omega \Phi_i(x)v(x)dx}{\int_\Omega \Phi_i(x)dx}, \; \forall x_i \in \mathcal{N}_c \tag{4.5}$$

In order to define interpolators for rough functions and to preserve piecewise polynomial boundary conditions, the approximated functions are averaged appropriately using (4.5) in order to generate nodal values for the interpolation operator.

Compare the dimension of the fine-scale space, we obtain that space V_f and the kernel space of the Clément-type interpolation operator $\mathcal{I}_H$ are equal. In addition, the solution space W has the orthogonal decomposition $W = kernel(\mathcal{I}_H) \oplus V_H = V_f \oplus V_H$ in $L^2(\Omega)$ sense. Namely, $\forall u \in W$, we have the decomposition $u = u_H + u_f$, where $u_H \in V_H$, $u_f \in V_f$, and they satisfy $(u_H, u_f)_{L^2(\Omega)} = 0$.

The Clément-type interpolation operators possess the local approximation and stability properties that are crucial in our error estimate. There exists a generic constant $C_{\mathcal{I}_H}$ such that for all $v \in W$ and for all coarse element $T_e \in \mathcal{T}_H$, we have

$$||v(x) - \mathcal{I}_H v(x)||_{L^2(T_e)} \leq C_{\mathcal{I}_H} H ||\nabla v(x)||_{L^2(S_e)}, \tag{4.6}$$

where $S_e := \cup \{K \in \mathcal{T}_H | K \cap T_e \neq \varnothing\}$ [7]. We also assume that there exists a constant $C_{ol} > 0$ such that the number of elements covered by S_e is uniformly bounded by C_{ol}. Both $C_{\mathcal{I}_H}$ and C_{ol} may depend on the shape regularity of the finite element mesh but not on the coarse mesh size H.

4.2 Quasi-orthogonal decomposition of the solution space

With these preparations, we are ready to study the structure of the generalized finite element space V_c (spanned by $\Psi_i(x)$) and the corresponding orthogonal decomposition of the solution space $W := H_0^1(\Omega)$. First, we explore the connections between the standard H^1 norm $\|\nabla \cdot\|_{L^2(\Omega)}$, norm $|||\cdot|||$, and the bilinear form $a(u,v)$. We get the following lemmas.

Lemma 4.1. *For any u,v in W, we have*

$$|a(u,v)| \lesssim |||u||| \, |||v|||.$$

Proof. Using the Cauchy-Schwarz inequality, we can obtain that

$$
\begin{aligned}
|a(u,v)|^2 &\leq (\|\nabla u\|_{L^2(\Omega)}\|\nabla v\|_{L^2(\Omega)} + V_0\|u\|_{L^2(\Omega)}\|v\|_{L^2(\Omega)}) \\
&\leq (\|\nabla u\|_{L^2(\Omega)}^2 + V_0\|u\|_{L^2(\Omega)}^2)(\|\nabla v\|_{L^2(\Omega)}^2 + V_0\|v\|_{L^2(\Omega)}^2) \\
&\leq |||u|||^2 |||v|||^2.
\end{aligned}
$$

$\square$

Lemma 4.2. $\|\nabla \cdot\|_{L^2(\Omega)}$ *and* $|||\cdot|||$ *are equivalent in* V_f, *given* $H\sqrt{V_0} \lesssim 1$.

Proof. For any w in V_f, $\|\nabla w\|_{L^2(\Omega)} \leq |||w|||$ is obvious. For the other direction,

$$
\begin{aligned}
|||w|||^2 &= (w - \mathcal{I}_H w, w - \mathcal{I}_H w)V_0 + (\nabla w, \nabla w) \\
&\leq V_0\|w - \mathcal{I}_H w\|_{L^2(\Omega)}^2 + (\nabla w, \nabla w) \\
&= V_0 \Big(\sum_{T \in \mathcal{T}_H} \|w - \mathcal{I}_H w\|_{L^2(\Omega)}^2 \Big) + (\nabla w, \nabla w) \\
&\leq H^2 V_0 C_{\mathcal{I}_H}^2 C_{ol} \|\nabla w\|_{L^2(\Omega)}^2 + \|\nabla w\|_{L^2(\Omega)}^2 \\
&= (H^2 V_0 C_{\mathcal{I}_H}^2 C_{ol} + 1)\|\nabla w\|_{L^2(\Omega)}^2 \lesssim \|\nabla w\|_{L^2(\Omega)}^2.
\end{aligned}
$$

$\square$

Lemma 4.3. *The bilinear form* $a(\cdot,\cdot)$ *is* V_f-*elliptic, given* $H\sqrt{V_0} < \frac{1}{C_{\mathcal{I}_H}\sqrt{C_{ol}}}$.

Proof. For any w in V_f, we have

$$
\begin{aligned}
a(w,w) &\geq -V_0\|w\|_{L^2(\Omega)}^2 + \|\nabla w\|_{L^2(\Omega)}^2 \\
&= -V_0\|w - \mathcal{I}_H w\|_{L^2(\Omega)}^2 + \|\nabla w\|_{L^2(\Omega)}^2 \\
&\geq (1 - H^2 V_0 C_{\mathcal{I}_H}^2 C_{ol})\|\nabla w\|_{L^2(\Omega)}^2 \\
&\geq \frac{1 - H^2 V_0 C_{\mathcal{I}_H}^2 C_{ol}}{1 + V_0 H^2 C_{\mathcal{I}_H}^2 C_{ol}} |||w|||_{\Omega}^2,
\end{aligned}
$$

where the last inequality directly follows from the previous lemma 4.3.

$\square$

In the Section 3, our new basis functions $\{\Psi_i(x)\}$ are constructed through an optimization problem. For any i, let $\Psi_i(x)$ be the unique minimizer of the following problem

$$\Psi_i(x) = \underset{\Psi(x) \in W}{\operatorname{argmin}} \quad a(\Psi, \Psi) \tag{4.7}$$

$$\text{s.t.} \int_\Omega \Psi(x)\Phi_j(x)dx = \delta_{i,j}. \tag{4.8}$$

Then, the generalized finite element space V_c is spanned by $\{\Psi_i(x)\}_{i=1}^{N_H}$. We shall show that for each i, the optimization problem (4.7)(4.8) gives rise to a minimizer $\Psi_i(x)$ given certain conditions. In addition, we shall show that the above optimization problem yields an orthogonal decomposition of the solution space W into the generalized finite element space V_c and its quasi-orthogonal complement V_f. Quasi-orthogonal decomposition means $\forall u \in W$, we have the decomposition $u = u_c + u_f$, where $u_c \in V_c$, $u_f \in V_f$, and they satisfy the condition $a(u_c, u_f) = 0$. We notice that relation $(f,g) = (\mathcal{H}\mathcal{H}^{-1}f, g) = a(\mathcal{H}^{-1}f, g)$, $\forall f, g \in W$ and the bilinear form $a(\cdot, \cdot)$ is symmetric. Therefore, the constrains $\int_\Omega \Psi \Phi_j = \delta_{i,j}$ in the optimization problem is equivalent to $a(\Psi, \mathcal{H}^{-1}\Phi_j) = \delta_{i,j}$. For each i, we define

$$W_i = \{\Psi(x) \in W | \int_\Omega \Psi(x)\Phi_j(x)dx = \delta_{i,j},\ j = 1,...,N_H\}$$

to be the *feasible set* of the optimization problem (4.7). Then, we have that

Lemma 4.4. *Under the resolution condition $H\sqrt{V_0} < \frac{1}{C_{\mathcal{I}_H}\sqrt{C_{ol}}}$, the optimization problem (4.7)(4.8) is a strictly convex optimization problem over W_i, for each i.*

Proof. Let us choose any two different $\Psi_a, \Psi_b \in W_i$. We write for $\eta \in [0,1]$,

$$f(\eta) = a(\Psi_a + \eta(\Psi_b - \Psi_a), \Psi_a + \eta(\Psi_b - \Psi_a))$$
$$= a(\Psi_a, \Psi_a) + 2\eta a(\Psi_a, \Psi_b - \Psi_a) + \eta^2 a(\Psi_b - \Psi_a, \Psi_b - \Psi_a).$$

Use the fact that $\Psi_b - \Psi_a \in V_f$ defined in (4.3) and $a(\cdot, \cdot)$ is V_f-elliptic by the Lemma 4.3, we get that $f''(\eta) > 0$. Thus, we finish the proof. $\qquad\square$

Lemma 4.5. *For any $1 \le i \le N_H$, the optimization problem (4.7)(4.8) has a minimizer $\Psi_i(x)$ if and only if $\{\mathcal{H}^{-1}\Phi_i\}_{i=1}^{N_H}$ are linearly independent.*

Proof. We define an N_H-by-N_H matrix Θ with $\Theta_{i,j} := (\mathcal{H}^{-1}\Phi_i, \Phi_j)$. It is clear that Θ is invertible if and only if $\{\mathcal{H}^{-1}\Phi_i\}_{i=1}^{N_H}$ are linearly independent. Let us define $\Psi_i(x) = \sum_{k=1}^{N_H} \Theta_{i,k}^{-1}\mathcal{H}^{-1}\Phi_k(x)$, where $\Theta_{i,k}^{-1}$ is the (i,k)-th entry of Θ^{-1}. It is easy to find that

$$\left(\sum_{k=1}^{N_H} \Theta_{i,k}^{-1}\mathcal{H}^{-1}\Phi_k, \Phi_j\right) = \sum_{k=1}^{N_H} \Theta_{i,k}^{-1}\Theta_{k,j} = \delta_{i,j},$$

which means that $\sum\limits_{k=1}^{N_H}\Theta_{i,k}^{-1}\mathcal{H}^{-1}\Phi_k$ satisfies the constrains (4.8). Thus linear independency of $\{\mathcal{H}^{-1}\Phi_i\}_{i=1}^{N_H}$ will imply existence of the minimizer. As for the other direction, assume that there exists a Ψ_i such that $a(\Psi_i,\mathcal{H}^{-1}\Phi_j)=\delta_{i,j}$, for all $j=1,2,...,N_H$. Suppose we have $\sum\limits_{j=1}^{N_H}\alpha_j\mathcal{H}^{-1}\Phi_j=0$. Then for each i, we will have that $0=\sum\limits_{j=1}^{N_H}\alpha_ja(\Psi_i,\mathcal{H}^{-1}\Phi_j)=\sum\limits_{j=1}^{N_H}\alpha_j\delta_{i,j}=\alpha_i$. Thus $\{\mathcal{H}^{-1}\Phi_j\}_{j=1}^{N_H}$ are linearly independent. $\qquad\square$

Lemma 4.6. *The optimization problem (4.7)(4.8) yields an orthogonal decomposition of the solution space W into the generalized finite element space V_c and its quasi-orthogonal complement V_f. Namely, $a(u_c,u_f)=0$, for any $u_c\in V_c$ and $u_f\in V_f$.*

Proof. Let Ψ_i be a minimizer. Then for any $w\in V_f$, we consider the objective function $a(\Psi_i+c\cdot w,\Psi_i+c\cdot w)$, $c\in R$. As Ψ_i satisfies the constrains, i.e. $\int_\Omega\Psi_i\Phi_j=\delta_{i,j}$, we also have $\int_\Omega(\Psi_i+c\cdot w)\Phi_j=\delta_{i,j}$, since w is orthogonal to every Φ_i according to (4.3). We define $m(c):=a(\Psi_i+c\cdot w,\Psi_i+c\cdot w)=c^2a(w,w)+2c\cdot a(\Psi_i,w)+a(\Psi_i,\Psi_i)$. Since $a(\cdot,\cdot)$ is V_f-elliptic by the Lemma 4.3, we have that $a(w,w)>0$ for nontrivial w. Recall that Ψ_i is a minimizer, we obtain that $m'(c)|_{c=0}=2a(\Psi_i,w)=0$, and this should holds for every $w\in V_f$. From the definition of V_c in (3.4), we get the conclusion that $a(u_c,u_f)=0$, for any $u_c\in V_c$ and $u_f\in V_f$.

To see that $W=V_c+V_f$, we firstly note that V_c is an N_H-dimensional subspace of W and that $V_c\cap V_f=0$ by definition. For any i in $\{1,2,\cdots,N_H\}$, write Ψ_i as $v_{f,i}+v_{H,i}$, where $v_{f,i}\in V_f$ and $v_{H,i}\in V_H$. Then, we can show that $\{v_{H,i}\}$ are linearly independent, because otherwise, there exists non-trivial c_i's such that $\sum\limits_i c_iv_{H,i}=0$, which implies that $\sum\limits_i c_i\Psi_i\in V_f$, a contradiction. Now, as $\{v_{H,i}\}$ are linearly independent, any element in V_H can be written as linear combination of Ψ_i's and an element in V_f. Thus, further, we can have $W=V_c+V_f$. $\qquad\square$

Remark 4.1. From Lemma 4.5 and Lemma 4.6, we can actually show that when $a(\cdot,\cdot)$ is a positive definite bilinear form, the minimizer has a simple form $\Psi_i=\sum\limits_{k=1}^{N_H}\Theta_{i,k}^{-1}\mathcal{H}^{-1}\Phi_k(x)$. See [16] for more details.

We also comment that V_c contains some fine-scale information of V_f which is very important in our computation of the eigenvalue problem. We shall show this in our error estimates and numerical experiments. The quasi-orthogonal decomposition with respect to $a(\cdot,\cdot)$ does not exactly preserve the L^2-orthogonality. However, we find that the error can be controlled.

Theorem 4.1. *For any $v_c\in V_c$ and $v_f\in V_f$, we have*

$$(v_c,v_f)_{L^2(\Omega)}\lesssim H^2|||\nabla v_c|||\,|||\nabla v_f|||. \tag{4.9}$$

Proof. For any $v_c \in V_c$ and $v_f \in V_f$, we have

$$(v_c, v_f)_{L^2(\Omega)} = (v_c - \mathcal{I}_H v_c, v_f - \mathcal{I}_H v_f)_{L^2(\Omega)} \lesssim H^2 \|\nabla v_c\|_{L^2(\Omega)} \|\nabla v_f\|_{L^2(\Omega)}$$
$$\lesssim H^2 |||v_c||| \, |||v_f|||$$

where we have used the fact $(\mathcal{I}_H v_c, v_f)_{L^2(\Omega)} = 0$, $\mathcal{I}_H v_f = 0$, and the stable estimate of the Clément-type interpolation (4.6). $\qquad\square$

Remark 4.2. In previous works [16, 20, 23], the authors utilized the Clément-type interpolation or optimization approach to upscale elliptic operators. The corresponding optimization problem is strictly convex over the solution space W. In our case, the Hamiltonian operator $-\Delta + V(x)$ may not be positive definite. Hence, the corresponding optimization problem is not strictly convex over the solution space W. Based on our numerical experiments and analysis, we found that under the assumption 4.1, we can prove that our optimization problem is strictly convex over W_i, which enables us to obtain the quasi-orthogonal decomposition of W and construct the basis functions Ψ_i for model reduction.

4.3   Exponential decay of the basis function Ψ_i

We shall show that the basis function Ψ_i decay exponentially fast away from its associated vertex $x_i \in \mathcal{N}_c$, namely the basis functions have exponential decay property. In practice, when we solve the optimization problem (4.7)(4.8) to construct the basis function Ψ_i, we choose a localized domain $S_i \subseteq \Omega$ associated with x_i and impose the condition that $supp\{\Psi_i\} \subseteq S_i$. Therefore, the exponential decay property significantly reduces our computational cost in constructing basis functions.

We first define a series of nodal patches Ω_l associated with $x_i \in \mathcal{N}_c$ by

$$\Omega_0 := supp\{\Phi_i\} = \cup\{K \in \mathcal{T}_H | x_i \in K\}, \tag{4.10}$$

$$\Omega_l := \cup\{K \in \mathcal{T}_H | K \cap \overline{\Omega_{l-1}} \neq \varnothing\}, \quad l = 1,2,3,4,\cdots. \tag{4.11}$$

Then, we state the main theorem as follows and put the detailed proof in the A.

Theorem 4.2. *Under the resolution condition $H\sqrt{V_0} < \frac{1}{2C_{\mathcal{I}_H}\sqrt{C_{ol}}}$, there exist some constants $C > 0$ and $0 < \beta < 1$ independent of H, such that*

$$\|\nabla\Psi_i\|_{\Omega\backslash\Omega_l} \leq C\beta^l \|\nabla\Psi_i\|_\Omega \tag{4.12}$$

for any $i = 1,2,...,N_H$.

The exponential decay of the basis functions Ψ_i allows us to localize the computational domain of the basis functions and to reduce the computational cost. In practice,

we modify the constrained optimization problem (3.2)(3.3) as follows,

$$\Psi_i(x) = \underset{\Psi \in H_0^1(\Omega)}{\arg\min} \int_\Omega \left(|\nabla \Psi(x)|^2 + V(x)|\Psi(x)|^2 \right) dx \tag{4.13}$$

$$\text{s.t.} \int_\Omega \Psi(x)\Phi_j(x) = \delta_{i,j}, \ \forall 1 \le j \le N_H, \tag{4.14}$$

$$\Psi(x) = 0, \ x \in \Omega \backslash \Omega_{l^*}. \tag{4.15}$$

where Ω_{l^*} is the support set of the basis function $\Psi_i(x)$ and l^* depends on the decay speed of $\Psi_i(x)$. In numerical experiments, we find that a small integer $l^* \sim \log(L/H)$ will generate accurate results, where L is the diameter of domain Ω. Moreover, the optimization problem (4.13)-(4.15) can be done in parallel.

4.4 Error estimate for the eigenvalues

In this subsection, we shall provide the error estimate of the eigenvalues $|\lambda_h - \lambda_H|$ obtained by the FEM and our new method. Before we proceed, we add an assumption that describes the well-posedness condition of the bilinear form $a(\cdot, \cdot)$.

Assumption 4.2. We assume that the bilinear form $a(\cdot, \cdot)$ satisfies

$$\inf_{u \in W \backslash \{0\}} \sup_{v \in W \backslash \{0\}} \frac{a(u,v)}{|||u|||\,|||v|||} \ge C > 0,$$

where the positive constant C may depend on V_0 and the domain Ω.

Let E_l denote the eigen-space spanned by the first l eigenfunctions obtained by the finite element method. $E_l := \text{span}\{u_h^{(1)}, \cdots, u_h^{(l)}\}$, where $u_h^{(i)}$'s are normalized to be one in $L^2(\Omega)$ norm. Recall that we have $\lambda_h^{(1)} \le \lambda_h^{(2)} \le \lambda_h^{(3)} \le \lambda_h^{(l)}$. Let $\lambda_h^* = \max_{1 \le i \le l}\{|\lambda_h^{(i)}|\}$. Then, we can estimate $|\lambda_h - \lambda_H|$ working in the eigen-space E_l.

Lemma 4.7. *Assume the assumption* (4.2) *is satisfied. For* $u \in E_l$ *with* $\|u\|_{L^2(\Omega)} = 1$ *and let* $u = u_c + u_f$ *be the quasi-orthogonal decomposition, where* $u_c \in V_c \bigcap E_l$ *and* $u_f \in V_f \bigcap E_l$. *Then, we have the following three estimates:*

$$|||u_c||| \lesssim l\lambda_h^*, \tag{4.16}$$

$$|||u_f||| \lesssim (l\lambda_h^*)^2 H^2, \tag{4.17}$$

$$|(u_c, u_f)| \lesssim (l\lambda_h^*)^3 H^4. \tag{4.18}$$

Proof. Let $u = \sum_{j=1}^{l} c_j u_h^{(j)}$, where c_j's are the projection coefficients of u on the eigenfunctions $u_h^{(j)}$ and $|c_j| \le 1$. According to the assumption (4.2), there exists $u_2 \in W \backslash \{0\}$, such that

$a(u,u_2) \gtrsim |||u|||\,|||u_2|||$. Then we have

$$|||u|||\,|||u_2||| \lesssim a(u,u_2) = a(\sum_{j=1}^{l} c_j u_h^{(j)}, u_2) = \sum_{j=1}^{l} c_j a(u_h^{(j)}, u_2)$$

$$= \sum_{j=1}^{l} c_j \lambda_h^{(j)}(u_h^{(j)}, u_2) \le l\lambda_h^* \|u_h^{(j)}\|\,\|u_2\| \le l\lambda_h^* |||u_2|||.$$

Thus, we have

$$|||u_c||| \le |||u||| \lesssim l\lambda_h^*.$$

We also have

$$|||u_f|||^2 \lesssim a(u_f, u_f) = a(u, u_f) = \sum_{j=1}^{l} c_j a(u_h^{(j)}, u_f) = \sum_{j=1}^{l} c_j \lambda_h^{(j)}(u_h^{(j)}, u_f)$$

$$\lesssim l\lambda_h^* H^2 |||u_h^{(j)}|||\,|||u_f||| \lesssim (l\lambda_h^*)^2 H^2 |||u_f|||.$$

The last inequality directly follows from (4.9) of Theorem 4.1 and the above two inequalities. $\qquad\square$

Finally, we estimate the error for the eigenvalues $|\lambda_h - \lambda_H|$ obtained by the FEM and our new method.

Theorem 4.3. *When the coarse mesh H is chosen small enough such that $H < 2^{-\frac{1}{4}}(l\lambda_h^*)^{-\frac{3}{4}}$. Then, we can get the following estimate*

$$\left|\frac{\lambda_H^{(l)} - \lambda_h^{(l)}}{\lambda_h^{(l)}}\right| \le (l\lambda_h^*)^2 H^4, \, l = 1, 2, \dots$$

Proof. Define $\sigma_H^{(l)} := \max_{u \in E_l:(u,u)=1} |(u_f, u_f)_{L^2(\Omega)} + 2(u_c, u_f)_{L^2(\Omega)}|$. Then, we have the following estimate for $\sigma_H^{(l)}$,

$$(u_f, u_f) + 2(u_c, u_f) = (u, u_f) + (u_c, u_f)$$
$$= (u - \mathcal{I}_H u, u_f - \mathcal{I}_H u_f) + (u_c, u_f)$$
$$\lesssim H^2 \|\nabla u\|_{L^2(\Omega)} \|\nabla u_f\|_{L^2(\Omega)} + (l\lambda_h^*)^3 H^4$$
$$\le H^2 |||u|||_\Omega |||u_f|||_\Omega + (l\lambda_h^*)^3 H^4$$
$$\lesssim (l\lambda_h^*)^3 H^4, \tag{4.19}$$

where we have used the fact that $|||u_f||| \lesssim (l\lambda_h^*)^2 H^2$. Therefore, we obtain that $\sigma_H^{(l)} \lesssim (l\lambda_h^*)^3 H^4$. If H is chosen small enough so that $\sigma_H^{(l)} \le 1/2$, i.e., $H \le 2^{-\frac{1}{4}}(l\lambda_h^*)^{-\frac{3}{4}}$. Then, Lemma 6.1 in [30] implies

$$\lambda_H^{(l)} \le (1 - \sigma_H^{(l)})^{-1} \lambda_h^{(l)} \le (1 + 2\sigma_H^{(l)}) \lambda_h^{(l)}$$

After some simple calculations, one can easily obtain the final result based on the estimate for $\sigma_H^{(l)}$ in (4.19). $\qquad\square$

5 Numerical Experiments

In this section, we conduct numerical experiments to illustrate our analytical results. More specifically, we will consider several different models of Schrödinger equations and test the performances of our method. Examples include Schrödinger equations of free electrons and those with double-well potentials. We are able to demonstrate that the relative error of eigenvalues converges of order at least $\mathcal{O}(H^4)$. Aside from the large convergence rate, using our problem dependent basis functions $\{\Psi_i\}$, we are able to achieve at a numerical method of better computational complexity than finite element method. Moreover, using our basis functions, one can capture the first few eigenvalue and eigenfunctions of stationary Schrödinger Equations accurately. The potentials taken in the examples are frequently used in chemistry models, which shows that our method is a very efficient model reduction method.

5.1 Hamiltonian of a free electron

In this example, we consider the Hamiltonian of a free electron in a bounded domain Ω with Dirichlet boundary condition. In our numerical experiments, $\mathcal{H} = -\partial_{xx}$ and the bounded domain Ω is taken to be $[0,1]$ for one dimensional problems. $\mathcal{H} = -\Delta$ and the bounded domain Ω is $[0,1]^2$ for two dimensional problems.

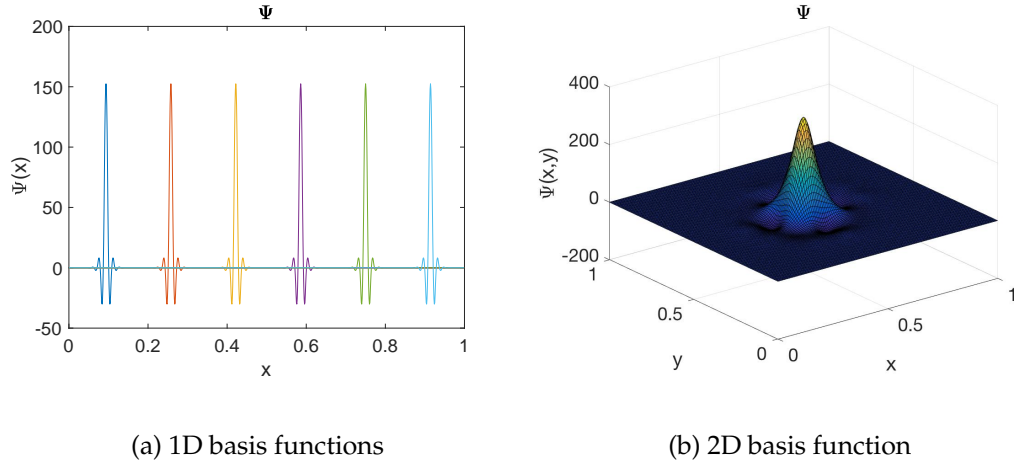(a) 1D basis functions

(b) 2D basis function

Figure 1: Profiles of the basis functions Ψ in 1D and 2D.

In 1D case, we uniformly partition our interval into $N_H = 128$ patches, and for each patch, we further uniformly partition it into $N_r = 8$ parts for numerical computation. We use the

Lagrange multiplier method to solve the optimization problem. Then, with the computed problem dependent basis functions, we discretize the Hamiltonian operator $\mathcal{H}$ onto the N_H-dimensional space spanned by $\Psi_1, \cdots, \Psi_{N_H}$ and approximate the smallest N_H eigenvalues of $\mathcal{H}$. In 2D case, we set the coarse mesh $H = \frac{1}{16}$ and partition our unit square into 256 squares (512 triangle elements). For each element, we further uniformly partition it into fine triangle element with mesh $h = \frac{1}{128}$. The computation method is similar.

In Figure 1, we plot the profiles of the basis functions obtained from our method. One can see that the basis functions decay exponentially fast, which numerically verify our proof on the exponential decay of the basis functions Ψ_i. Therefore, we can localize the computational domain of the basis functions and reduce the computational cost. Due to the exponential decay of the basis functions, we can maintain a certain level of accuracy using the localized basis functions.
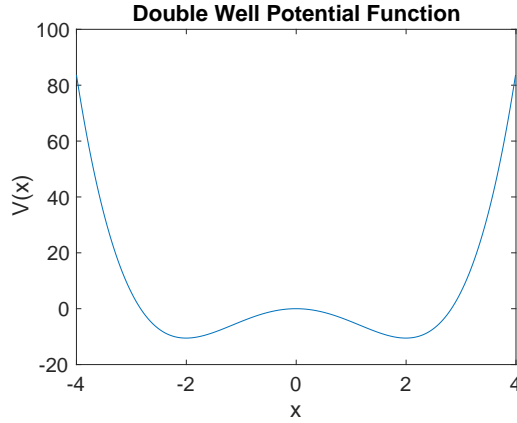

Figure 2: Profile of the double well potential function

5.2   1D Schrödinger equations with double well potential

Another model problem we consider is Schrödinger equations with double well potential [12,22,28], which can be used to model the proton motion restricted to the line joining the two bridged atoms separated by a fixed distance. The stationary Schrödinger equation in this case can be formulated as

$$u''(\xi) + \frac{1}{2}(E' - V')u(\xi) = 0, \tag{5.1}$$

where $E = \frac{1}{4}\hbar\beta E'$, $V = \frac{1}{4}\hbar\beta V'$, $\xi = \alpha x$, $\alpha = (\mu\beta\hbar)^{\frac{1}{2}}$, $\hbar$ is the reduced Planck constant, μ is the reduced mass of the H bond A-H$\cdots$B, and β is an arbitrary frequency. We suppose also that the potential energy of the proton can be represented as a polynomial in the proton coordinate x. On the basis of both experimental and theoretical investigations, it is generally assumed that the potential-energy surface of many hydrogen bonds has two

l	$\lambda_h^{(l)}$	$e^{(l)}(1/4)$	$e^{(l)}(1/8)$	$e^{(l)}(1/16)$	$e^{(l)}(1/32)$
1	-7.4193719518	1.3835941155	0.0038910332	0.0000818444	0.0000028630
2	-7.4112857508	1.9049638409	0.0090247237	0.0000823858	0.0000028577
3	-2.1299632024	1.0847454244	0.0228617229	0.0000653230	0.0000255027
4	-1.7356348046		0.0370931918	0.0000594389	0.0000437861
5	1.5265029050		0.0443342756	0.0000731927	0.0000671185
6	3.7596565522		0.2392715598	0.0006789233	0.0000539193
7	6.8680570735		0.0785633586	0.0021042608	0.0000391890
8	10.2397336594			0.0051750133	0.0000235955
9	13.9262761972			0.0137490946	0.0000071148
10	17.8750209804			0.0359595248	0.0000642540
11	22.0630278538			0.0550625298	0.0001634628
12	26.4710403941			0.0283996294	0.0003259629
13	31.0847265155			0.0520077439	0.0005803314
14	35.8938813732			0.3381533790	0.0009646512
15	40.8927032420			0.1824533435	0.0015294094

Table 1: Relative errors $e_H^{(l)} = \left| \frac{\lambda_H^{(l)} - \lambda_h^{(l)}}{\lambda_h^{(l)}} \right|$ for $l = 1, \cdots 15$, potential function being $V(x)$, and various choices of the coarse mesh size H. Space means no available data.

minima in the region available for protonic movement [28]. In most cases the minima are not equivalent since the physical situation is changed when the proton is transferred from one minimum to the other.

We consider the interval $[-4, 4]$ and partition it into $N_H = 4, 8, 16, 32$ patches respectively and further partition them such that the partition number of the fine mesh is $N_h = 1024$. Our potential function is taken to be $V(x) = -5.26x^2 + 0.6575x^4$ and its graph is plotted in Figure 2 .

In the Table 1, we compare the eigenvalues $\lambda_h^{(l)}$ obtained through finite element method with the eigenvalues $\lambda_H^{(l)}$ obtained on coarse-scale approximations using problem-dependent basis functions with different mesh size H. The chart illustrates that the convergence rate of relative error is at least of order $\mathcal{O}(H^4)$, which matches our analysis.

We have also run some tests to compare the errors of the approximated eigenfunctions. In Figure 3, one can find that the eigenfunctions obtained from our method can capture the reference eigenfunctions accurately. Especially, note that the double well potentials take negative values at some x. This indicates the operator $\mathcal{L}$ is no longer positive semidefinite. Even in this case, our method can still accurately approximate the first few eigenfunctions of the Schrödinger equation.

As in the Figure 3, qualitatively, we can see that the graph of approximated eigenfunctions computed through our method overlap with that of the fine-scale finite element

(a) First eigenfunction

(b) Second eigenfunction

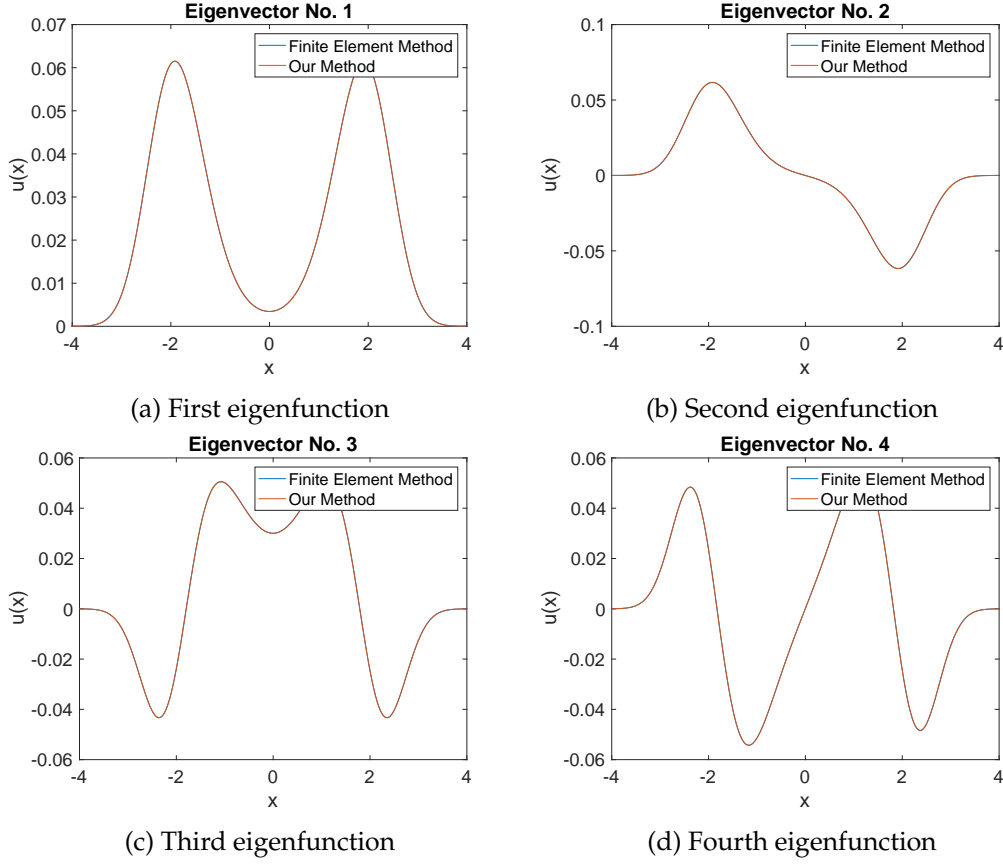(c) Third eigenfunction

(d) Fourth eigenfunction

Figure 3: Selected examples of computed eigenfunctions using our method as compared to eigenfunctions obtained through finite element method in fine scale.

method. In the Table 2, we show the relatively error $\frac{\|u_H^{(l)} - u_h^{(l)}\|_{L^2(\Omega)}}{\|u_h^{(l)}\|_{L^2(\Omega)}}$, $l = 1, 2, \ldots$. One can see that the relative errors are very small, which indicates that our method can accurately compute the eigenfunctions.

To demonstrate the computational savings of the our method over the finite element method, we show in Figure 4 the computational time of compute first 15 eigenvalues and eigenfunctions of the Schrödinger equation. Based on our previous result in Table 1, we assume that if the coarsening ratio is 64, then the relative error $|\frac{\lambda_H^{(l)} - \lambda_h^{(l)}}{\lambda_h^{(l)}}| < 1\%$. We choose $N_h = 2^{11}, 2^{12}, 2^{13}, 2^{14}, 2^{15}$, and $N_H = 2^5, 2^6, 2^7, 2^8, 2^9$, respectively. We record the wall time of running the eigenvalue algorithm in Matlab. From the Figure 4, one can see that our new method offers considerable savings over the finite element method. The slope of the blue line with stars is approximate equal to 2.56, which means the computational complexity of eigenvalue algorithm is $O(N_h^{2.56})$. The complexity of our method is also in the similar

order $O(N_H^\alpha)$ with $\alpha \approx 2.5$, but N_H is far less than N_h. Therefore, our method can bring significant savings over the FEM. The advantage of our method will be more obvious in two or higher dimensional problems.

We should point out that in this example we choose the coarsening ratio to be 64, which is used to demonstrate the main idea. In general, this ratio is problem-dependent and may be different. However, considerable savings over the finite method can always be achieved if we only compute first few eigenvalues and eigenfunctions of the Schrödinger equation because our method can efficiently reduce the dimension of the problem. Here we only compare the wall time of running the eigenvalue algorithm. In the FEM, one needs extra time to form the large-scale stiffness and mass matrices. In our method, we need extra time to compute the problem dependent basis functions, which is not a serious issue as this can be done in parallel.

l	$e^{(l)}(1/4)$	$e^{(l)}(1/8)$	$e^{(l)}(1/16)$	$e^{(l)}(1/32)$	$e^{(l)}(1/64)$
1	0.6965984460	0.0774389135	0.0060291238	0.0057078965	0.0057077218
2	0.6965984460	0.0774389135	0.0060291238	0.0057078965	0.0057077218
3	0.6965984460	0.0774389135	0.0060291238	0.0057078965	0.0057077218
4		0.3248398972	0.0103391321	0.0073621435	0.0073601873
5		1.4082343730	0.0189615168	0.0084268470	0.0084164228
6		1.4082343730	0.0189615168	0.0084268470	0.0084164228
7		0.2068980702	0.0189615168	0.0084268470	0.0084164228
8			0.0337396932	0.0095348370	0.0094984863
9			0.0711299849	0.0105979475	0.0104960909

Table 2: Errors $e^{(l)}(H) =: \frac{\|u_H^{(l)} - u_h^{(l)}\|_{L^2(\Omega)}}{\|u_h^{(l)}\|_{L^2(\Omega)}}$ for $l = 1, \cdots 9$, potential function being $V(x)$ and various coarse mesh sizes H. Space means no available data.

5.3   2D Schrödinger equations with double well potential

In 2D problems, we consider the double well potential again, which can be used to mimic the nuclear attraction potential generated by two separate nuclei. Our computational domain is unit square $\Omega = [0,1]^2$. We partition Ω into $2N_H^2 = 8, 32, 128, 512$ right triangular elements respectively and further partition them such that the length of the fine-scale triangular elements remains to be $1/128$. In this setting, the fine-scale finite element space contains 32768 triangular elements. The potential function is taken to be $V(x) = -e^{(-100((x-\frac{1}{3})^2 + (y-\frac{1}{3})^2))} - e^{(-100((x-\frac{2}{3})^2 + (y-\frac{2}{3})^2)))}$ and its profile is plotted in the Figure 5.

In the Table 3, we compare the eigenvalues $\lambda_H^{(l)}$ obtained through our method on coarse scale with mesh size H and $\lambda_h^{(l)}$ obtained through finite element method on fine mesh. The chart illustrates that the convergence rate of relative error is at least of order $\mathcal{O}(H^4)$, which matches our analysis.
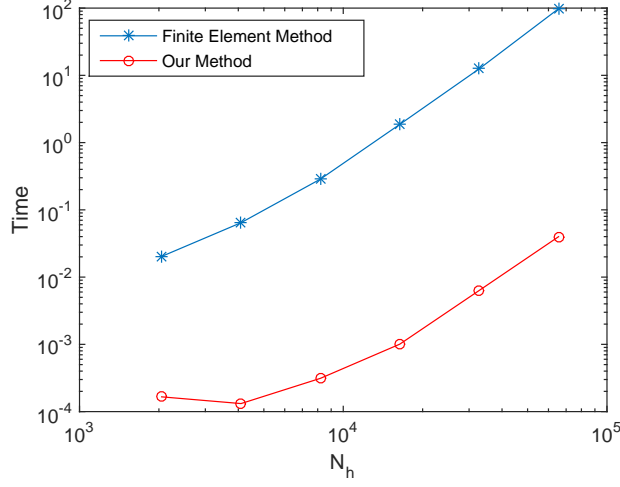
Figure 4: Computational time comparison. The slope of the blue line with stars is approximately equal to 2.56.

l	$\lambda_h^{(l)}$	$e^{(l)}\left(\frac{1}{2}\right)$	$e^{(l)}\left(\frac{1}{4}\right)$	$e^{(l)}\left(\frac{1}{8}\right)$	$e^{(l)}\left(\frac{1}{16}\right)$
1	19.6091772610	0.0219784613	9.8340489578	0.0000692656	0.0000177255
2	49.1412025030		1.9911925433	0.0004530679	0.0000540041
3	49.3430613108		1.7657226037	0.0003209520	0.0000490705
4	78.8921013458		0.2945283689	0.0010193662	0.0000952112
5	98.6998638157		0.0301345748	0.0015716893	0.0001298963
6	98.7015416394		0.1830111746	0.0015720886	0.0001298952
7	128.3476681238		0.6136893299	0.0022049449	0.0001681032
8	128.4018950402		0.6152620757	0.0034741934	0.0002184742
9	167.7715860381		0.8830349576	0.0047696354	0.0002968372
10	167.9116924534			0.0047105112	0.0002936821
11	177.8715926909			0.0059546459	0.0003294618
12	197.5146060216			0.0072691230	0.0003944581
13	197.6078861306			0.0073017043	0.0003936524
14	247.0403560121			0.0099947299	0.0004769060
15	247.2626621136			0.0157984022	0.0007181437

Table 3: Relative errors of eigenvalues $e^{(l)}(H) =: \frac{\lambda_H^{(l)} - \lambda_h^{(l)}}{\lambda_h^{(l)}}$ for $l = 1, \cdots 15$, potential function being $V(x)$ and various choices of the coarse mesh size H. Space means no available data.

We have also run some tests on approximated eigenfunctions. In Figure 6, we see that our method can approximate the first few eigenfunctions of the Schrödinger equation
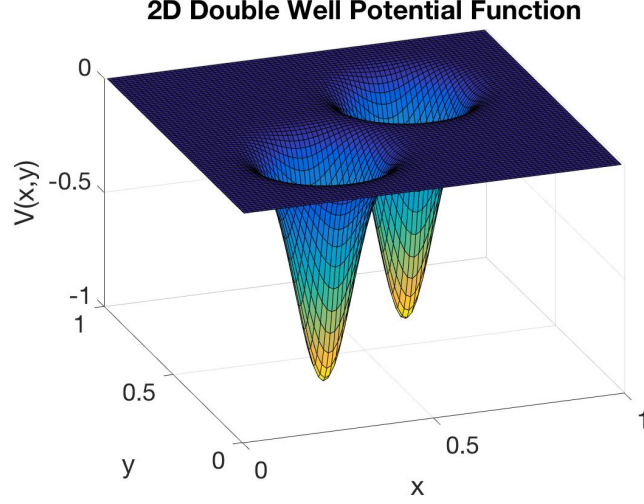
Figure 5: Profile of the 2D double well potential function

accurately. Especially, note that the double well potentials take negative values at some x. This indicates the operator $\mathcal{L}$ is no longer positive semidefinite. Even in this case, our method can still approximate the first few eigenfunctions of the Schrödinger equation accurately.

As shown in the figure 6, qualitatively, we can see that the graph of approximated eigenfunctions computed through our method overlap with that of the fine-scale finite element method. Here, the domain is taken to be $[0,1]^2$ and we partition the unit square into $2m^2 = 512$ right triangular patches respectively and further partition them into 16 parts. Quantitatively, the relatively errors $\frac{\|u_H^{(l)} - u_h^{(l)}\|_{L^2(\Omega)}}{\|u_h^{(l)}\|_{L^2(\Omega)}}$, $l = 1,2,...$, are kept at a very low level, indicating the accuracy of our method in capturing the first few eigenfunctions, where $u_H^{(l)}$ stand for eigenfunctions computed through our method and $u_h^{(l)}$ stand for eigenfunctions computed through finite element method.

$e^{(1)}$	$e^{(4)}$	$e^{(7)}$
0.000253557665	0.000964396658	0.000154570260

Table 4: Relative errors of eigenfunctions $e^{(l)} := \frac{\|u_H^{(l)} - u_h^{(l)}\|_{L^2(\Omega)}}{\|u_h^{(l)}\|_{L^2(\Omega)}}$ for $l=1,4,7$ potential function being $V(x)$, the coarse mesh size H is $1/16$, and the fine mesh size $h = 1/128$.

5.4 A simple study of choosing coarse mesh size H

We shall investigate how the course mesh size H is scaled with the fine mesh size h in order to keep the error rate at a similar level. We consider the one dimensional free electron model as discussed in Section 5.1. Since true eigenvalues $\lambda_{\text{TRUE}}^{(l)}$ of this model problem can be computed analytically, we compare the relative errors of $|e_H^{(l)}| = |\frac{\lambda_H^{(l)} - \lambda_{\text{TRUE}}^{(l)}}{\lambda_{\text{TRUE}}^{(l)}}|$ and $|e_h^{(l)}| = |\frac{\lambda_h^{(l)} - \lambda_{\text{TRUE}}^{(l)}}{\lambda_{\text{TRUE}}^{(l)}}|$, where $\lambda_H^{(l)}$ are computed using our new basis functions and $\lambda_h^{(l)}$ are computed using finite element basis function with mesh size indicated in the bracket.

In table 5, we compared the differences between two types of relative errors obtained through our method and finite element method respectively. For each pair of relative errors, we fix the mesh size to be $H = h^{1/2}$ and consider the errors incurred when computing the first few eigenvalues. We can see from the table that relatively errors are at the same level. This provides us with an empirical guidance on how to choosing coarse mesh size H. More theoretical and numerical investigations of our method will be considered in our subsequent research.

l	$|e_H^{(l)}(1/16)|$	$|e_h^{(l)}(1/16^2)|$	$|e_H^{(l)}(1/32)|$	$|e_h^{(l)}(1/32^2)|$	$|e_H^{(l)}(1/64)|$	$|e_h^{(l)}(1/64^2)|$
1	0.0000125478	0.0000125499	0.0000007843	0.0000007844	0.0000000490	0.0000000490
2	0.0000500623	0.0000502004	0.0000031355	0.0000031375	0.0000001961	0.0000001961
3	0.0001112512	0.0001129538	0.0000070365	0.0000070593	0.0000004409	0.0000004412
4	0.0001900937	0.0002008137	0.0000124177	0.0000125499	0.0000007824	0.0000007844
5	0.0002667773	0.0003137856	0.0000190841	0.0000196093	0.0000012181	0.0000012256
6	0.0002873505	0.0004518762	0.0000265911	0.0000282375	0.0000017422	0.0000017648
7	0.0001217994	0.0006150938	0.0000340436	0.0000384345	0.0000023443	0.0000024021

l	$|e_H^{(l)}(1/128)|$	$|e_h^{(l)}(1/128^2)|$	$|e_H^{(l)}(1/256)|$	$|e_h^{(l)}(1/256^2)|$
1	0.0000000031	0.0000000030	0.0000000002	0.0000000006
2	0.0000000123	0.0000000122	0.0000000008	0.0000000008
3	0.0000000276	0.0000000276	0.0000000017	0.0000000017
4	0.0000000490	0.0000000490	0.0000000031	0.0000000031
5	0.0000000765	0.0000000766	0.0000000048	0.0000000048
6	0.0000001100	0.0000001103	0.0000000069	0.0000000069
7	0.0000001493	0.0000001501	0.0000000094	0.0000000094

Table 5: Relative errors of $|e_H^{(l)}| = |\frac{\lambda_H^{(l)} - \lambda_{\text{TRUE}}^{(l)}}{\lambda_{\text{TRUE}}^{(l)}}|$ and $|e_h^{(l)}| = |\frac{\lambda_h^{(l)} - \lambda_{\text{TRUE}}^{(l)}}{\lambda_{\text{TRUE}}^{(l)}}|$, $l = 1, \cdots 7$ for the free electron model with various choices of the coarse mesh size H and fine mesh size h. Space means no available data.

6 Conclusions

In this paper, we propose a model reduction method to construct problem dependent basis functions and compute eigenvalues and eigenfunctions of stationary Schrödinger equations. The basis function are obtained through solving an optimization problem. Under mild conditions, we prove that the generalized finite element space spanned by our basis functions can accurately compute the first few eigenvalues and eigenfunctions of the stationary Schrödinger equations. In addition, our new method can significantly reduce the computational cost in eigenvalue decomposition problems compared with the standard finite element method on fine mesh. We demonstrate through numerical experiments to show that our method works well for Schrödinger equations with double well potentials, in which case the differential operators are no longer positive semidefinite.

There are several directions we want to explore in our future work. Firstly, we would like to construct problem dependent basis functions to compute eigenvalues and eigenfunctions of Schrödinger equations with unbounded potential, such as Coulomb potential. Then, we would like to employ our new basis functions to compute time-evolutionary Schrödinger equations. In addition, we shall construct problem dependent basis functions using optimization approach to solve problems arising from uncertainty quantification, such as multiscale elliptic PDEs with random coefficients.

7 Acknowledgements

A Exponential decay of the basis function Ψ_i

In this appendix, we provide a detailed derivation of the Theorem 4.2. For the ease of reading, we state the theorem again as follows,

Theorem A.1. *Under the resolution condition* $H\sqrt{V_0} < \frac{1}{2C_{\mathcal{I}_H}\sqrt{C_{ol}}}$, *there exist some constant* $C > 0$ *and* $0 < \beta < 1$ *independent of H, such that*

$$||\nabla\Psi_i||_{\Omega\setminus\Omega_l} \leq C\beta^l ||\nabla\Psi_i||_\Omega \tag{A.1}$$

for any $i = 1,2,...,N_H$.

Proof. To facilitate the proof, we make use of a few properties of the Clément-type interpolation operator $\mathcal{I}_H$. For more detailed arguments, we refer the interested readers to

Section 6 of [7]. Note that there exists a constant $C_{\mathcal{I}_H}$ such that, for all $v \in V$ and $x_i \in \mathcal{N}_c$,

$$H^{-1}\|v - \mathcal{I}_H v\|_{L^2(\Omega_0)} + \|\nabla(v - \mathcal{I}_H v)\|_{L^2(\Omega_0)} \leq C_{\mathcal{I}_H}\|\nabla v\|_{L^2(\Omega_1)}. \tag{A.2}$$

The constant $C_{\mathcal{I}_H}$ depends on the shape regularity parameter γ but does not depend on the local mesh size H.

Notice that $\mathcal{I}_H|_{V_H}$ is a local operator, by which we mean it gives rise to a sparse matrix, but its inverse $(\mathcal{I}_H|_{V_H})^{-1}$ is not. Nevertheless, there exists some bounded right inverse $\mathcal{I}_H^{-1,loc} : V_H \to V$ of $\mathcal{I}_H$ that is local. That is, there exists a constant $C'_{\mathcal{I}_H}$ depending only on γ, such that for all $v_H \in V_H$,

$$\begin{cases} \mathcal{I}_H(\mathcal{I}_H^{-1,loc} v_H) &= v_H, \\ \|\nabla \mathcal{I}_H^{-1,loc} v_H\|_\Omega &\leq C'_{\mathcal{I}_H}\|\nabla v_H\|_\Omega, \\ \mathrm{Supp}(\mathcal{I}_H^{-1,loc} v_H) &\subset \bigcup\{T_e \,|\, T_e \in \mathcal{T}_H : T_e \cap \overline{\mathrm{Supp}(v_H)} \neq \varnothing\}. \end{cases} \tag{A.3}$$

The third condition simply means that $\mathrm{Supp}(\mathcal{I}_H^{-1,loc} v_H)$ is included $\mathrm{Supp}(v_H)$ union another layer of coarse elements. More detailed results can be found in [21, 26].

Now we are in the position to prove the decay property of the basis function Ψ_i. The main idea of the proof is based on some iterative Caccioppoli-type argument that has been used in [16, 21, 26]. We define a projection operator $P : W \to V_f$ such that $a(Pv, w) = a(v, w)$ for any $v \in W$ and $w \in V_f$. More superficially, $Pv = \sum_{T \in \mathcal{T}_H} P_T(v|_T)$ and $P_T(v|_T)$ solves the equation $a(P_T(v|_T), w) = a_T(v, w)$ for all $w \in V_f$, where $a_T(\cdot, \cdot)$ means the restriction of the weak form $a(\cdot, \cdot)$ on the element T.

Now for any $x_i \in \mathcal{N}_c$, we define $P_i := \sum_{T \in \Omega_{i,0}} P_T(\Phi_i|_T)$ where $\Omega_{i,0} = \mathrm{Supp}(\Phi_i)$. And we shall prove the P_i has exponential decay property. To simplify notation, we omit the dependence on i and use Ω_0 to denote $\Omega_{i,0}$. We choose an integer l with $l \geq 7$ and define a cutoff function as $\eta(x) = \frac{\mathrm{dist}(x, \Omega_{l-4})}{\mathrm{dist}(x, \Omega_{l-4}) + \mathrm{dist}(x, \Omega \backslash \Omega_{l-3})}$, $x \in \Omega$. It is easy to check that the cutoff function $\eta(x)$ has the following properties: (1) $\eta = 0$ in Ω_{l-4}, (2) $\eta = 1$ in $\Omega \backslash \Omega_{l-3}$, (3) $0 \leq \eta \leq 1$, and η is Lipschitz continuous with $\|\nabla \eta\|_{L^\infty(\Omega)} \leq H^{-1}\gamma$, where γ depends on shape regularity parameter γ of the finite element triangles $\mathcal{T}_H$. Then we have the estimate

$$\begin{aligned} \|\nabla P_i\|_{\Omega \backslash \Omega_{l-3}} &= (\nabla P_i, \nabla P_i)_{\Omega \backslash \Omega_{l-3}} \\ &\leq (\nabla P_i, \eta \nabla P_i)_\Omega = (\nabla P_i, \nabla(\eta P_i))_\Omega - (\nabla P_i, (\nabla \eta) P_i)_\Omega \\ &\leq |(\nabla P_i, \nabla(\eta P_i - \mathcal{I}_H^{-1,loc}(\mathcal{I}_H(\eta P_i))))_\Omega| + |(\nabla P_i, \nabla(\mathcal{I}_H^{-1,loc}(\mathcal{I}_H(\eta P_i))))_\Omega| \\ &\quad + |(\nabla P_i, (\nabla \eta) P_i)_\Omega|. \end{aligned} \tag{A.4}$$

To simplify notations, we define

$$\begin{aligned} M_1 &:= |(\nabla P_i, \nabla(\eta P_i - \mathcal{I}_H^{-1,loc}(\mathcal{I}_H(\eta P_i))))_\Omega|, \\ M_2 &:= |(\nabla P_i, \nabla(\mathcal{I}_H^{-1,loc}(\mathcal{I}_H(\eta P_i))))_\Omega|, \\ M_3 &:= |(\nabla P_i, (\nabla \eta) P_i)_\Omega|. \end{aligned}$$

From the definition of $\mathcal{I}_H$ in (4.4), we know that $\mathcal{I}_H(\eta P_i - \mathcal{I}_H^{-1,loc}(\mathcal{I}_H(\eta P_i)))_\Omega = 0$. This implies that $\eta P_i - \mathcal{I}_H^{-1,loc}(\mathcal{I}_H(\eta P_i)) \in V_f$ with support in $\Omega \backslash \Omega_{l-6}$. Thus, $\eta P_i - \mathcal{I}_H^{-1,loc}(\mathcal{I}_H(\eta P_i))$ vanishes on Ω_0 as long as $l \geq 6$ and we have $a(v, \eta P_i - \mathcal{I}_H^{-1,loc}(\mathcal{I}_H(\eta P_i)))_{\Omega_0} = 0$ for any v in W. Then, we have

$$
\begin{aligned}
M_1 &= |(\nabla P_i, \nabla(\eta P_i - \mathcal{I}_H^{-1,loc}(\mathcal{I}_H(\eta P_i))))_\Omega| \\
&= |(V P_i, \eta P_i - \mathcal{I}_H^{-1,loc}(\mathcal{I}_H(\eta P_i)))_\Omega| \\
&\leq V_0 |(P_i, \eta P_i - \mathcal{I}_H^{-1,loc}(\mathcal{I}_H(\eta P_i)))_\Omega|.
\end{aligned}
$$

Note that $\eta P_i - \mathcal{I}_H^{-1,loc}(\mathcal{I}_H(\eta P_i))$ is supported in $\Omega \backslash \Omega_{l-6}$, so when $l \geq 6$, it vanishes on Ω_0. Using the properties of (A.2)(A.3), arguments used in Lemma 4.2, and the resolution condition , we have

$$
\begin{aligned}
M_1 &\leq V_0 |(P_i, \eta P_i - \mathcal{I}_H^{-1,loc}(\mathcal{I}_H(\eta P_i)))_\Omega| \\
&\leq C_{\mathcal{I}_H}^2 C_{ol} H^2 V_0 \|\nabla P_i\|^2_{\Omega \backslash \Omega_{l-6}} + C_{\mathcal{I}_H}^3 C'_{\mathcal{I}_H} C_{ol} H^2 V_0 \|\nabla P_i\|^2_{\Omega_l \backslash \Omega_{l-7}} \\
&\leq \tfrac{1}{2} \|\nabla P_i\|^2_{\Omega \backslash \Omega_l} + \tfrac{1}{2}(1 + C_{\mathcal{I}_H} C'_{\mathcal{I}_H}) \|\nabla P_i\|^2_{\Omega_l \backslash \Omega_{l-7}}.
\end{aligned}
\tag{A.5}
$$

Similar techniques and the Lipschitz bound lead to upper bounds of M_2 and M_3,

$$
\begin{aligned}
M_2 &\leq C'_{\mathcal{I}_H} C_{\mathcal{I}_H} \|\nabla(\eta P_i)\|_{\Omega_{l-1} \backslash \Omega_{l-6}} \|\nabla P_i\|_{\Omega_{l-1} \backslash \Omega_{l-6}} \\
&\leq C'_{\mathcal{I}_H} C_{\mathcal{I}_H} \left(C_{\mathcal{I}_H} \sqrt{C_{ol}} \|H \nabla \eta\|_{L^\infty(\Omega)} + 1 \right) \|\nabla P_i\|^2_{\Omega_l \backslash \Omega_{l-7}}
\end{aligned}
\tag{A.6}
$$

and

$$
M_3 \leq C_{\mathcal{I}_H} \sqrt{C_{ol}} \|H \nabla \eta\|_{L^\infty(\Omega)} \|\nabla P_i\|^2_{\Omega_{l-2} \backslash \Omega_{l-5}}.
\tag{A.7}
$$

The combination of estimates (A.5)-(A.7) yields

$$
\tfrac{1}{2} \|\nabla P_i\|^2_{\Omega \backslash \Omega_l} \leq C_1 \|\nabla P_i\|^2_{\Omega_l \backslash \Omega_{l-7}},
$$

where $C_1 := \tfrac{1}{2} + \tfrac{3}{2} C_{\mathcal{I}_H} C'_{\mathcal{I}_H} + (C'_{\mathcal{I}_H} C_{\mathcal{I}_H} + 1) C_{\mathcal{I}_H} \sqrt{C_{ol}} \gamma$ depends only on the shape regularity γ of the finite element triangles $\mathcal{T}_H$. Since $\|\nabla P_i\|^2_{\Omega_l \backslash \Omega_{l-7}} = \|\nabla P_i\|^2_{\Omega \backslash \Omega_{l-7}} - \|\nabla P_i\|^2_{\Omega \backslash \Omega_l}$, we have the contraction

$$
\|\nabla P_i\|^2_{\Omega \backslash \Omega_l} \leq \frac{C_1}{C_1 + \tfrac{1}{2}} \|\nabla P_i\|^2_{\Omega \backslash \Omega_{l-7}}.
$$

Finally, some algebraic calculations yield the exponential decay of the P_i's,

$$
\|\nabla P_i\|^2_{\Omega \backslash \Omega_l} \leq \left(\frac{C_1}{C_1 + \tfrac{1}{2}} \right)^{\left\lfloor \frac{l}{7} \right\rfloor} \|\nabla P_i\|^2_\Omega.
\tag{A.8}
$$

After proving that P_i's decay exponentially, we shall show that Ψ_i's have the some property. Notice that by definition, $P_i - \Phi_i \in V_c$ and moreover, they span the space V_c. Thus

each Ψ_i can be written as a linear combination of $P_i - \Phi_i$'s, namely, $\Psi_i = \sum_j a_j^{(i)} (P_j - \Phi_j)$, for some coefficients $a_j^{(i)}$. And from the condition that $(\Psi_i, \Phi_k) = \delta_{i,k}$, we have that $(\sum_j a_j^{(i)} (P_j - \Phi_j), \Phi_k) = \delta_{i,k}$. Thus $\sum_j a_j^{(i)} (\Phi_j, \Phi_k) = -\delta_{i,k}$. Let M be an $N_H \times N_H$ mass matrix with entry (Φ_i, Φ_k) and write $a^{(i)} = (a_1^{(i)}, \cdots, a_{N_H}^{(i)})^T$. Then $M a^{(i)} = -e_i$, where e_i is a column vector with i-th entry equals to one and other entries equal 0, and thus $a^{(i)} = -M^{-1} e_i$.

If we number the finite element basis functions Φ_i in a proper way, so that the mass M is a banded matrix with bandwidth at most p. Then we know that the entries of M^{-1} has the decay property

$$|(M^{-1})_{ij}| \leq 2\rho^{2|i-j|/p} ||M^{-1}||_2, \tag{A.9}$$

where $\rho = (\sqrt{\mathrm{cond}_2(M)} - 1)/(\sqrt{\mathrm{cond}_2(M)} + 1)$. See Theorem 4.8 in [3] for more details. Thus, $a_j^{(i)}$ decays exponentially away from $a_i^{(i)}$. Now as each $P_j - \Phi_j$ decays exponentially, their exponentially-decay linear combination also decays exponentially. Recall that $\Psi_i = \sum_j a_j^{(i)} (P_j - \Phi_j)$, now take $\beta = \max\{\rho^{2/p}, \left(\frac{C_1}{C_1 + \frac{1}{2}}\right)^{\frac{1}{7}}\}$, then we get the exponential decay property for Ψ_i, namely,

$$||\nabla \Psi_i||^2_{\Omega \setminus \Omega_l} \leq C \beta^l ||\nabla \Psi_i||^2_\Omega.$$

$\square$

We remark that when Φ_i's are taken to be piecewise constant basis functions as proposed in [16], their correspond mass matrix M reduces to a diagonal matrix and thus $a_j^{(i)} = \delta_{ij}$. In this case, $\Psi_i = a_i^{(i)} (P_i - \Phi_i)$ and its exponential decay property follows trivially from the decay property of P_i.

References

[1] I. Babuska, G. Caloz, and E. Osborn. Special finite element methods for a class of second order elliptic problems with rough coefficients. *SIAM J. Numer. Anal.*, 31:945–981, 1994.

[2] I. Babuška and J. Osborn. Eigenvalue problems. *Handbook of numerical analysis*, 2:641–787, 1991.

[3] M. Bebendorf. *Hierarchical Matrices: A Means to Efficiently Solve Elliptic Boundary Value Problems*, volume 212. Springer Berlin Heidelberg, 2008.

[4] S. Boyd and L. Vandenberghe. *Convex optimization*. Cambridge university press, 2004.

[5] S. Brenner and R. Scott. *The mathematical theory of finite element methods*, volume 15. Springer Science & Business Media, 2007.

[6] Laurie J Butler. Chemical reaction dynamics beyond the Born-Oppenheimer approximation. *Annual review of physical chemistry*, 49(1):125–171, 1998.

[7] C. Carstensen and R. Verfürth. Edge residuals dominate a posteriori error estimates for low order finite element methods. *SIAM journal on numerical analysis*, 36(5):1571–1587, 1999.

[8] M. Cheng, T. Y. Hou, M. Yan, and Z. Zhang. A data-driven stochastic method for elliptic PDEs with random coefficients. *SIAM J. UQ*, 1:452–493, 2013.

[9] P. H. Clément. Approximation by finite element functions using local regularization. *Revue française d'automatique, informatique, recherche opérationnelle. Analyse numérique*, 9(R2):77–84, 1975.

[10] James W. Demmel. *Applied numerical linear algebra*. Society for Industrial and Applied Mathematics, 1997.

[11] Y. R. Efendiev, T. Y. Hou, and X. Wu. Convergence of a nonconforming multiscale finite element method. *SIAM Journal on Numerical Analysis*, 37(3):888–910, 2000.

[12] M.D. Feit, J.A. Fleck, and A. Steiger. Solution of the Schrödinger equation by a spectral method. *Journal of Computational Physics*, 47(3):412–433, 1982.

[13] W. Hackbusch. On the computation of approximate eigenvalues and eigenfunctions of elliptic operators by means of a multi-grid method. *SIAM journal on numerical analysis*, 16(2):201–215, 1979.

[14] T. Y. Hou and X. Wu. A multiscale finite element method for elliptic problems in composite materials and porous media. *J. Comput. Phys.*, 134:169–189, 1997.

[15] T. Y. Hou, X. Wu, and Z. Cai. Convergence of a multiscale finite element method for elliptic problems with rapidly oscillating coefficients. *Mathematics of Computation*, 68(227):913–943, 1999.

[16] T. Y. Hou and P. Zhang. Sparse operator compression of elliptic operators part 1: second order elliptic operators. Submitted.

[17] S. Jin, P. Qi, and Z. Zhang. An Eulerian surface hopping method for the Schrödinger equation with conical crossings. *SIAM Multiscale Model. Simul.*, 9:258–281, 2011.

[18] T. Kato. On the eigenfunctions of many-particle systems in quantum mechanics. *Communications on Pure and Applied Mathematics*, 10(2):151–177, 1957.

[19] R. Kosloff and H Tal-Ezer. A direct relaxation method for calculating eigenfunctions and eigenvalues of the schrödinger equation on a grid. *Chemical physics letters*, 127(3):223–230, 1986.

[20] A. Malqvist and D. Peterseim. Localization of elliptic multiscale problems. *Mathematics of Computation*, 83(290):2583–2603, 2014.

[21] A. Malqvist and D. Peterseim. Computation of eigenvalues by numerical upscaling. *Numerische Mathematik*, 130:337–361, 2015.

[22] G.J. Milburn, J. Corney, E.M. Wright, and D.F. Walls. Quantum dynamics of an atomic bose-einstein condensate in a double-well potential. *Physical Review A*, 55(6):4318, 1997.

[23] H. Owhadi. Bayesian numerical homogenization. *SIAM Multiscale Model. Simul.*, 13(3):812–828, 2015.

[24] V. Ozoliņš, R. Lai, R. Caflisch, and S. Osher. Compressed modes for variational problems in mathematics and physics. *Proceedings of the National Academy of Sciences*, 110(46):18368–18373, 2013.

[25] V. Ozoliņš, R. Lai, R. Caflisch, and S. Osher. Compressed plane waves yield a compactly supported multiresolution basis for the Laplace operator. *Proceedings of the National Academy of Sciences*, 111(5):1691–1696, 2014.

[26] D. Peterseim. Eliminating the pollution effect in Helmholtz problems by local subscale correction. *Mathematics of Computation*, 86(305):1005–1036, 2017.

[27] L. Scott and S. Zhang. Finite element interpolation of nonsmooth functions satisfying boundary conditions. *Mathematics of Computation*, 54(190):483–493, 1990.

[28] R. Lo. Somorjai and D.F. Hornig. Double-minimum potentials in hydrogen-bonded solids.

The Journal of Chemical Physics, 36(8):1980–1987, 1962.

[29] H. Spohn and S. Teufel. Adiabatic decoupling and time-dependent Born-Oppenheimer theory. *Communications in Mathematical Physics*, 224(1):113–132, 2001.

[30] G. Strang and G. J. Fix. *An analysis of the finite element method*, volume 212. Prentice-hall Englewood Cliffs, NJ, 1973.

[31] J. G. Sun and A. H. Zhou. *Finite element methods for eigenvalue problems*. CRC Press, 2016.

[32] J. A. C. Weideman and L. N. Trefethen. The eigenvalues of second-order spectral differentiation matrices. *SIAM Journal on Numerical Analysis*, 25(6):1279–1298, 1988.

[33] J. Xu and A. Zhou. A two-grid discretization scheme for eigenvalue problems. *Math. Comput.*, 70(233):17–25, 2001.

[34] Z. Zhang, M. Ci, and T. Y. Hou. A multiscale data-driven stochastic method for elliptic PDEs with random coefficients. *SIAM Multiscale Model. Simul.*, 13:173–204, 2015.

[35] Z.M. Zhang. How many numerical eigenvalues can we trust? *Journal of Scientific Computing*, 65(2):455–466, 2015.
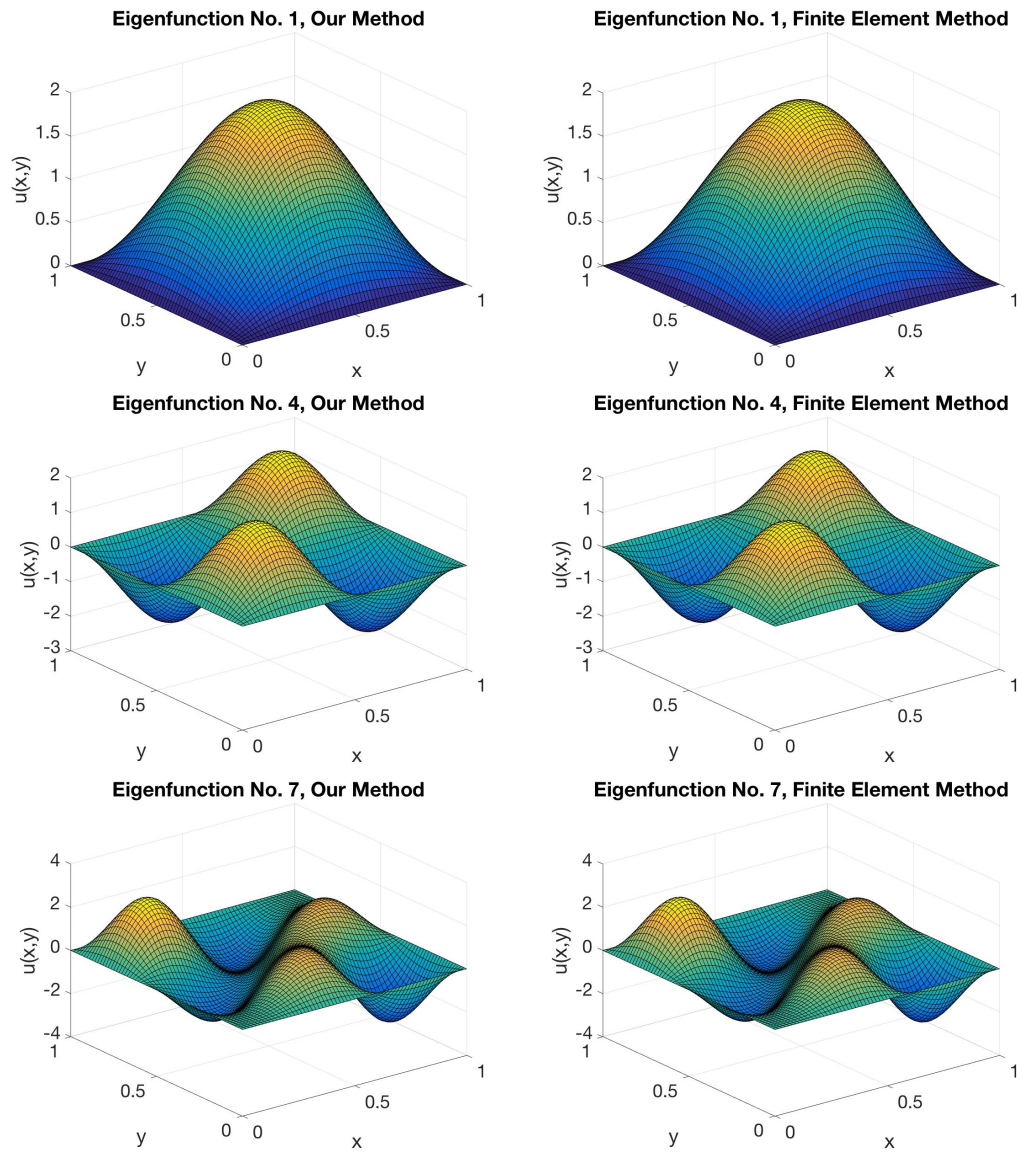
Figure 6: Selected examples of computed eigenfunctions as compared to eigenfunctions obtained through finite element method in fine scale.